

All (Rod) Amacrine Cells Form a Network of Electrically Coupled Interneurons in the Mammalian Retina

Margaret Lin Veruki and Espen Hartveit¹

University of Bergen

Department of Anatomy and Cell Biology

Årstadveien 19

N-5009 Bergen

Norway

Summary

All (rod) amacrine cells in the mammalian retina are reciprocally connected via gap junctions, but there is no physiological evidence that demonstrates a proposed function as electrical synapses. In whole-cell recordings from pairs of All amacrine cells in a slice preparation of the rat retina, bidirectional, nonrectifying electrical coupling was observed in all pairs with overlapping dendritic trees (average conductance ~ 700 pS). Coupling displayed characteristics of a low-pass filter, with no evidence for amplification of spike-evoked electrical postsynaptic potentials by active conductances. Coincidence detection, as well as precise temporal synchronization of subthreshold membrane potential oscillations and TTX-sensitive spiking, was commonly observed. These results indicate a unique mode of operation and integrative capability of the network of All amacrine cells.

Introduction

In the retina, amacrine cells constitute a heterogeneous population of local-circuit inhibitory interneurons. There is increasing evidence that these interneurons share common properties with local-circuit interneurons in other areas of the CNS, including the presence of gap junctions between cells of the same type. For several types of interneurons, morphological evidence for the existence of gap junctions was established decades ago, but the functional characteristics of the corresponding electrical synapses have remained elusive (reviewed by Galarreta and Hestrin, 2001). In the mammalian retina, All (rod) amacrine cells receive excitatory glutamatergic input from rod bipolar cells (reviewed by Masland, 2001). All amacrine cells are presynaptic to OFF-cone bipolar cells and they are connected by gap junctions to the axon terminals of ON-cone bipolar cells. These gap junctions are thought to be important for the transmission of scotopic signals from rod bipolar cells to retinal ganglion cells. In addition, however, the All amacrine cells are themselves interconnected by gap junctions at their arboreal dendrites in the inner plexiform layer (Kolb and Famiglietti, 1974). These anatomical findings pose a series of important questions. Do the gap junctions between All amacrine cells serve as a substrate for electrical communication, i.e., as electrical synapses? What would the functional significance of such synapses be? For example, is the junction conduc-

tance high enough that action potentials can be transmitted from one cell to another? Are putative electrical synapses between All amacrine cells able to synchronize spiking of coupled cells? Simultaneous dual recording, arguably the only direct and most convincing way to demonstrate electrical coupling (Galarreta and Hestrin, 2001), has, until now, been missing. In this study, we have recorded from pairs of visually identified All amacrine cells in *in vitro* slices of rat retina. Our results indicate the presence of strong electrical coupling among these retinal interneurons and the ability of this coupling to tightly synchronize both subthreshold membrane potential fluctuations and spike firing.

Results

Identification of All Amacrine Cells in Retinal Slices

All amacrine cells were targeted for recording according to the size and location of the cell body in the inner nuclear layer and the thick primary dendrite descending into the inner plexiform layer (Figure 1A, top). Cells were filled with Lucifer yellow and at the end of each recording, fluorescence microscopy allowed visualization of both cells' complete morphology, including lobular appendages and arboreal dendrites (Figure 1A, bottom).

Electrical Coupling of All Amacrine Cells

After establishing the whole-cell configuration in a pair of All amacrine cells, we tested for electrical coupling by applying voltage commands to one cell and recording the responses in both cells. A cell is henceforth referred to as presynaptic when it is the cell in which an experimental manipulation is initiated and as postsynaptic when it responds to a membrane potential change in the presynaptic cell (cf. Nolan et al., 1999). Application of a hyperpolarizing voltage step evoked an inward current in the presynaptic cell and when cells were electrically coupled, it also evoked an outward current in the postsynaptic cell (Figures 1B and 1C). Application of a depolarizing voltage step evoked an outward current in the presynaptic cell and an inward current in the postsynaptic cell (Figures 1B and 1C). In current clamp, a current step in the presynaptic cell evoked a presynaptic and postsynaptic voltage change of the same polarity, as expected for transmission via electrical synapses (Figures 1D and 1E). To isolate the effects of electrical coupling from chemical synaptic transmission, recordings were performed in the presence of antagonists of chemical neurotransmitters (see Experimental Procedures). In addition, where appropriate, experiments were repeated in control solution without antagonists in order to verify that the results obtained did not depend on the absence of chemical synaptic transmission as such. Coupling was not blocked by recording in extracellular solution with low Ca^{2+} /high Mg^{2+} or by replacing Ca^{2+} in the extracellular solution with an equivalent concentration of Co^{2+} . For all cell pairs, the electrical coupling was reciprocal (Figures 1B–1E).

¹Correspondence: espen.hartveit@iac.uib.no

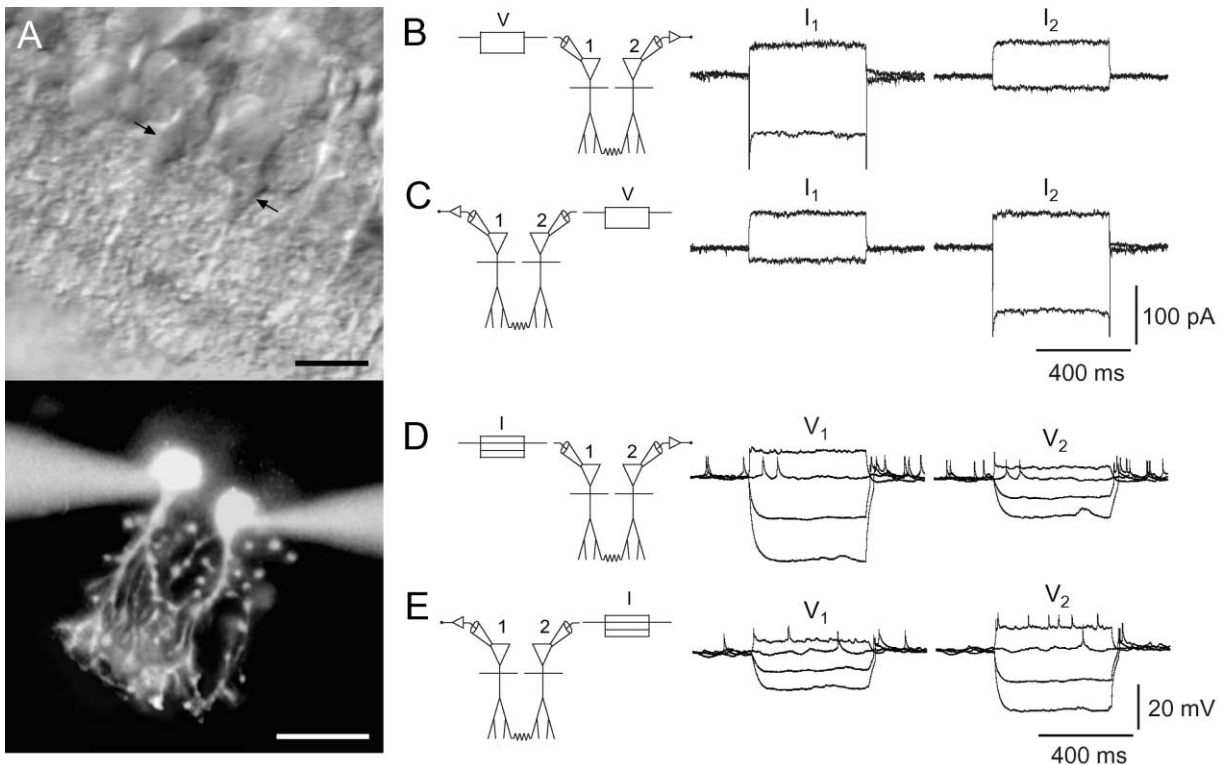


Figure 1. Simultaneous Recordings from Two All Amacrine Cells Reveal Bidirectional Electrical Coupling

(A) *Top*: a pair of All amacrine cells (marked by arrows) in a slice from rat retina, visualized with infrared differential interference contrast videomicroscopy. *Bottom*: composite fluorescence photomicrograph of same cell pair after filling with Lucifer yellow. Scale bars 20 μm .

(B) With a pair of All amacrine cells in voltage clamp ($V_h = -60$ mV), 500 ms voltage steps (V) of -30 mV and $+10$ mV are applied to cell 1 while current responses are recorded from both cells (I_1 and I_2). A hyperpolarizing pulse applied to cell 1 results in an inward current in cell 1 and an outward current in cell 2. A depolarizing pulse in cell 1 results in an outward current in cell 1 and an inward current in cell 2.

(C) Same as in (B), but voltage steps are applied to cell 2.

(D) With both cells in current clamp, 500 ms current pulses (I) of -50 , -25 , 0 , and $+25$ pA are applied to cell 1 while voltage responses are recorded from both cells (V_1 and V_2). Injection of negative current results in hyperpolarization of both cells and injection of positive current results in depolarization of both cells.

(E) Same as in (D), but the current pulses are applied to cell 2.

A total of 61 All amacrine cell pairs displayed electrical coupling identified as described above. Following fluorescence microscopy and visualization with Lucifer yellow, all but three pairs were observed to be in potential physical contact with each other as judged by overlap between the arboreal dendrites. Additionally, 11 All amacrine cell pairs did not display electrical coupling and subsequently, following visualization, were found to have non-overlapping dendritic trees. The mean distance between the somata of coupled cell pairs was 24 ± 1.1 μm (range 9–53 μm) while the mean distance between noncoupled pairs was 41 ± 3.7 μm (range 20–58 μm). As is the case, we also recorded from cell pairs in which only one cell was subsequently identified as an All amacrine cell. Electrical coupling was never observed between such cell pairs.

Electrical Junction Conductance

The junction conductance (G_j) was estimated with both cells in voltage clamp by applying a series of voltage commands to the presynaptic cell and recording the evoked currents in both the pre- and the postsynaptic cell (Figure 2A). The junction current (I_j) versus junction voltage (V_j) relationship, corrected for nonzero series

resistance and finite membrane input resistance, was linear (Figure 2B), indicating that G_j was independent of V_j over the range of voltages tested (± 30 mV). Accordingly, G_j was measured as the slope of a straight line fitted to the I - V relation (1.16 nS; Figure 2B). The junctional conductance was very similar for both directions of coupling (Figure 2C) and the conductance for a cell pair was calculated as the average of the conductance determined from each direction of coupling. The mean G_j (for cell pairs with potential physical contact) was 704 ± 76 pS ($n = 22$ cell pairs; range 310–1460 pS). For the three coupled cell pairs without overlapping arboreal dendrites, the G_j was very low (92, 154, and 207 pS) and we assume that the cells in these pairs were coupled via another cell.

Coupling Coefficient

A coupling coefficient was estimated as the ratio of the voltage change in the non-injected cell to that in the injected cell with both cells in current clamp. The mean steady state coupling coefficient (for cell pairs with potential physical contact) was 0.29 ± 0.03 ($n = 25$ cell pairs; range 0.11–0.65). Coupling coefficients could also be estimated for two of the coupled cell pairs without

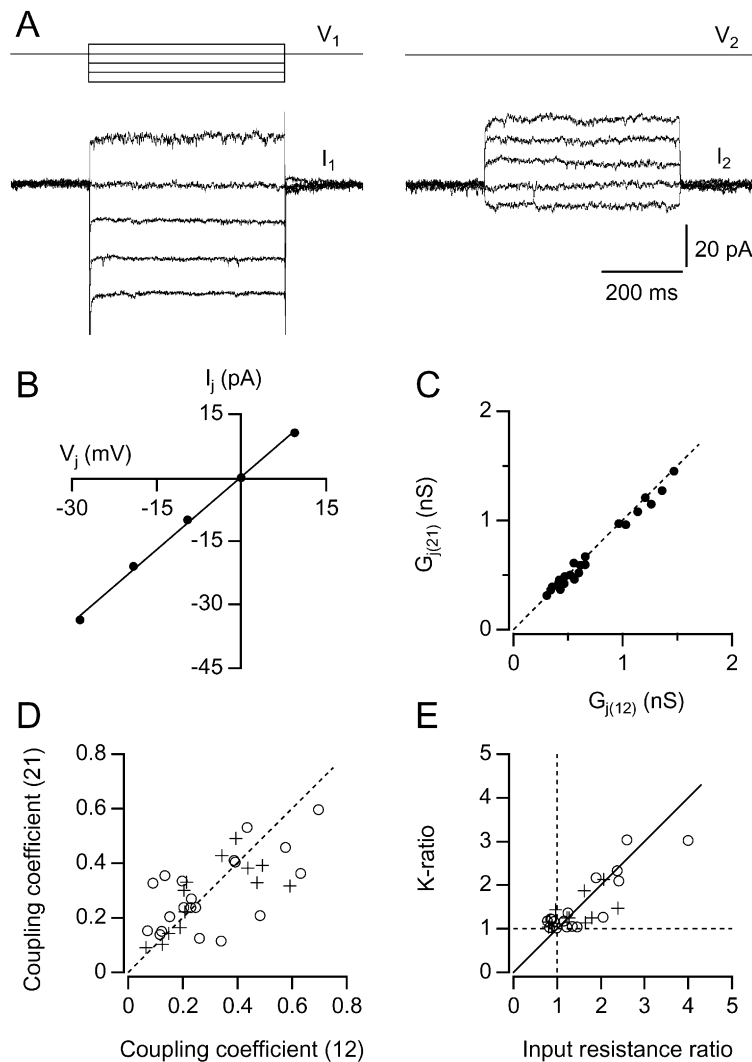


Figure 2. Estimation of Junctional Conductance (G_j) and Coupling Coefficient between Electrically Coupled Cells

(A) With both cells in voltage clamp (V_1 and V_2), voltage steps (-30 to $+10$ mV, 10 mV increments) were applied to one cell (V_1) and current responses were recorded in both cells (I_1 and I_2).

(B) Current-voltage relationship for the junctional current (I_j) versus the junctional voltage (V_j). The data points have been fit with a straight line (slope = G_j).

(C) Comparison of G_j in each direction indicates nonrectifying electrical coupling ($G_{j(12)}$ for cell 1 presynaptic, $G_{j(21)}$ for cell 2 presynaptic). The dashed line has a slope of one ($G_{j(12)} = G_{j(21)}$).

(D) Comparison of coupling coefficient in each direction indicates apparent rectification for some cell pairs (12 for cell 1 presynaptic, 21 for cell 2 presynaptic). Crosses (+): cell pairs in control condition; open circles (○): cell pairs in the presence of pharmacological blockers of chemical synaptic transmission. The dashed line has a slope of one (the values expected when the coupling coefficient is the same in both directions).

(E) Relation between apparent rectification (K-ratio; ratio of the higher to the lower coupling coefficient for a pair of cells) and input resistance ratio (calculated in the direction of the larger coupling coefficient). Symbols as in (D). The continuous line represents the values expected when pairs of cells are connected by asymmetrical coupling coefficients and input resistances, but symmetrical G_j . The horizontal and vertical dashed lines represent values expected when pairs of cells have identical coupling coefficients and input resistances, respectively.

overlapping arboreal dendrites and were 0.07 and 0.08 . For each cell pair, the coupling coefficient was estimated for both directions of coupling and the population average was calculated from the average for each pair. The scatterplot shown in Figure 2D indicates that the coupling coefficient was moderately asymmetric when the two directions of coupling were compared. The apparent rectification was quantified as the K-ratio, i.e., the ratio of the higher to the lower coupling coefficient for each cell pair (mean 1.6 ± 0.13 ; Nolan et al., 1999). This contrasts with the symmetrical junction conductance which cannot account for the apparent rectification (Figure 2C). An alternative explanation for the asymmetrical coupling coefficient is a difference in membrane input resistance between the two coupled cells. For a given presynaptic voltage change, the coupling coefficient will increase with increasing postsynaptic membrane resistance. We investigated this by plotting the K-ratio for each coupled pair against the ratio of membrane input resistance (Figure 2E). The latter ratio was calculated as the ratio of the postsynaptic to the presynaptic cell in the direction of the larger coupling coefficient. The result suggests that the asymmetry of cou-

pling coefficients can be accounted for by the difference in membrane input resistance.

Because pharmacological blocking of spontaneous postsynaptic currents might increase the postsynaptic membrane input resistance, and thereby the coupling coefficient, we repeated the measurements in control solution without antagonists. There was a weak, but not statistically significant, increase of membrane input resistance after blocking synaptic transmission pharmacologically (from 458 ± 43 to 487 ± 47 M Ω ; $n = 12$; $p = 0.29$; paired t test). The mean steady state coupling coefficient was 0.32 ± 0.03 ($n = 12$ cell pairs; range 0.14 – 0.45 ; Figure 2D), not significantly different from the coupling coefficient during blocked chemical synaptic transmission ($p = 0.50$). The mean K-ratio for cell pairs recorded in control solution was 1.4 ± 0.10 (Figure 2E).

Frequency Dependence of Electrical Synaptic Transmission

Electrical coupling between nerve cells can have the functional characteristics of a low-pass filter (Galarreta and Hestrin, 1999; Gibson et al., 1999; Nolan et al., 1999). We investigated this by recording from pairs of All ama-

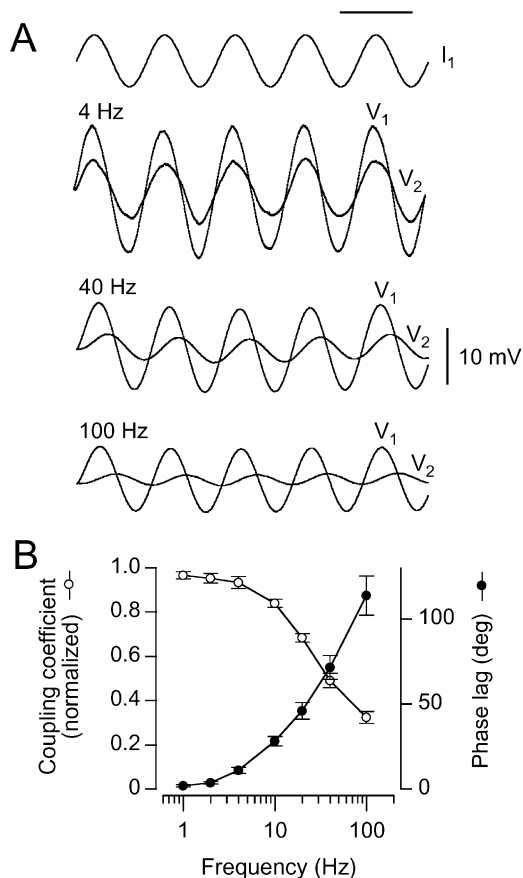


Figure 3. Electrical Coupling Displays Characteristics of a Low-Pass Filter

(A) Increasing phase lag and response attenuation between the voltage oscillations evoked in the presynaptic (V_1) and postsynaptic (V_2) cells of a coupled pair when injecting sinusoidal current stimuli (I_1 ; 100 pA peak-to-peak amplitude) of increasing frequency in the presynaptic cell (each trace is the average of 3–9 sweeps). Horizontal calibration bar indicates duration of one stimulus period (250 ms for 4 Hz, 25 ms for 40 Hz, and 10 ms for 100 Hz).

(B) Bode plot showing frequency dependence of response attenuation (coupling coefficient normalized to steady state coupling coefficient) and phase lag of sinusoidal voltage response in 11 electrically coupled cell pairs.

crine cells in current clamp and applying sinusoidal current stimuli of varying frequencies (1–100 Hz; Figure 3A). Action potentials were blocked by addition of TTX (Boos et al., 1993). For each frequency, we calculated the coupling coefficient and the phase shift. The phase shift was calculated by crosscorrelating the postsynaptic response with the presynaptic response and converting the temporal delay to phase by multiplying with $2\pi/T$, where T is the period of the stimulus. For each frequency, the coupling coefficient was normalized to the coupling coefficient for steady state responses in the same cell pair. The signal transmission has clear low-pass characteristics with increasing attenuation and phase shift for increasing stimulus frequency (Figure 3B).

Facilitation of Synchronous Spiking

One function of coupling of neurons by electrical synapses is synchronization of spiking. The spontaneous

firing rate of All amacrine cells recorded in control solution varied between 1 and 41 Hz with an average of 12 ± 3 Hz ($n = 16$, cells that did not fire spontaneously were not included). In several simultaneous recordings from pairs of All amacrine cells, synchronization of spontaneous spiking could be easily identified (Figure 4A). We investigated this synchronization quantitatively by calculating crosscorrelation histograms of simultaneously recorded spike trains in pairs of cells. The spike cross-correlograms typically displayed a sharp peak near zero time delay. In the example illustrated in Figure 4B (recorded in control solution), the central peak is clearly above the upper 99% confidence limit of the correlogram. The synchronization width was 4 ms and the synchronization strength was 7.1 (see Experimental Procedures). Similar crosscorrelograms with strong synchronization of spiking were seen in 6 of 7 cell pairs. The average synchronization strength was 11.4 ± 5.1 (range 2.4–35.5) and the average synchronization width was 7.2 ± 1.5 ms (range 3–13 ms), indicating a tight synchronization of spiking. In some cell pairs, the crosscorrelogram peak was located to one side of time zero (Figure 4B). For other cell pairs, we observed a crosscorrelogram with two peaks, one on each side of time zero. The average time delay of the (major) peak was 4.6 ± 1.2 ms (range 1.7–8.3 ms). We did not observe crosscorrelograms where a single peak was symmetrically distributed around time zero.

As synchronized firing may be caused by common chemical synaptic input, we recorded from cell pairs after blocking chemical synaptic transmission pharmacologically. The spontaneous firing rate of these cells was not significantly different from that of cells recorded in control solution (mean rate 19 ± 3 Hz, range 3–53 Hz, $n = 33$; $p = 0.23$). For nine cell pairs, the average synchronization strength was 13.1 ± 4.2 (range 2.1–31.6), the average synchronization width was 4.7 ± 0.9 ms (range 1–10 ms), and the average time delay was 4.3 ± 0.7 ms (range 1.8–7.4 ms). There was no statistically significant difference between these parameters for cell pairs recorded in control solution and cell pairs recorded in the presence of antagonists ($p > 0.15$). This suggests that the synchronization of firing is independent of chemical synaptic transmission.

Electrical Postsynaptic Potentials

The temporally precise correlation of spike generation in pairs of All amacrine cells suggests that spikes can be transmitted through electrical synapses between the recorded cells (cf. Galarreta and Hestrin, 1999; Gibson et al., 1999; Mann-Metzer and Yarom, 1999; Nolan et al., 1999; Tamás et al., 2000; Bartos et al., 2001). In several electrically coupled cell pairs, we observed that spontaneous action potentials in the presynaptic cell evoked slow depolarizations in the postsynaptic cell (Figure 5A). There were no failures. Figure 5B shows a series of traces with postsynaptic depolarizations (2) aligned by a spike in the presynaptic cell (1; same pair as Figure 5A). For this pair, the postsynaptic depolarizations had an average amplitude of 3.7 ± 0.05 mV (range 2.6–5.0 mV; $n = 121$ responses), a 10%–90% risetime of 3.3 ± 0.06 ms (range 2.2–5.2 ms), a latency from the presynaptic spike of 0.5 ± 0.008 ms (range 0.24–0.77

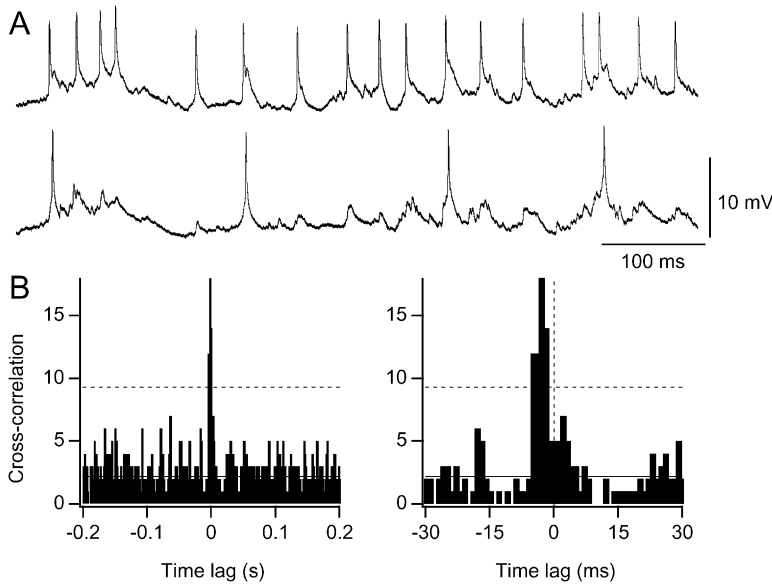


Figure 4. Synchronous Spiking in Electrically Coupled All Amacrine Cells

(A) Simultaneous voltage records from a pair of electrically coupled All amacrine cells (in control solution).

(B) Spike crosscorrelogram (1 ms bin width) for the cell pair in (A) at two different time scales. Dashed horizontal lines represent the 99% upper confidence limit. Continuous horizontal lines represent the expected level of correlation. Vertical dashed line (right) represents zero time delay.

ms), and a half-width (width at 50% of the peak amplitude) of 9.8 ± 0.1 ms (range 6.8–13.7 ms). The latency was determined as the time interval between the maximum slope of the presynaptic action potential (measured as the peak of the first derivative of that waveform) and the onset of the postsynaptic depolarization (measured as 5% of the peak amplitude). The low variability of the postsynaptic waveform parameters and the absence of failures suggest that the connection was monosynaptic and that the depolarizations corresponded to electrical postsynaptic potentials (electrical PSPs). The average coupling coefficient (ratio between the amplitude of the postsynaptic depolarization and the amplitude of the presynaptic spike) was 0.19. As expected, due to frequency-dependent attenuation, this was lower than the steady state coupling coefficient between the same cells which was 0.44. Similar observations and quantitative measurements of electrical PSPs were made for 14 additional cell pairs. The mean peak amplitude was 1.6 ± 0.4 mV (range 0.3–4.5 mV), the mean 10%–90% risetime was 3.8 ± 0.7 ms (range 0.9–10.6 ms), and the mean latency from the presynaptic spike was 0.5 ± 0.1 ms (range 0.06–1.6 ms). The mean coupling coefficient was 0.15 ± 0.03 (range 0.03–0.40).

In several cases, the depolarization evoked by a presynaptic spike reached threshold for spike generation in the postsynaptic cell (Figure 5C; arrows). In these cases, the latency from the presynaptic spike to the postsynaptic spike displayed larger variability than the latency from the presynaptic spike to the postsynaptic subthreshold depolarization (Figure 5D). When the postsynaptic cell generated a spike, it evoked a “reciprocal” postsynaptic depolarization in the original presynaptic cell (Figures 5C and 5E). In several cases, this depolarization evoked an additional spike (Figure 5C; arrowhead) which again evoked an electrical PSP in the original postsynaptic cell. We never observed further reverberatory firing.

Although we only recorded from pairs of All amacrine cells, we sometimes observed indirect evidence for

electrical coupling to other cells, making it likely that electrical coupling encompasses a more extensive network of All amacrine cells. In the example shown in Figure 5F, two electrically coupled cells received correlated subthreshold depolarizations, presumably caused by a small number of spiking cells connected independently to both cells recorded from. Some of the postsynaptic depolarizations displayed time courses similar to those described above. Whenever one of the cells recorded from reached threshold for spike firing, a corresponding electrical PSP was observed in the other cell.

Electrotonic versus Active Signal Transmission between Coupled Cells

These results strongly suggest that spikes can be reliably transmitted through electrical synapses between All amacrine cells and raise two important questions concerning the involvement of voltage-gated currents, specifically I_{Na} . First, is the spike-evoked electrical PSP generated by passive, electrotonic spread of depolarization from the presynaptic cell, or do postsynaptic voltage-gated currents contribute to its amplitude and time course? Second, do voltage-gated currents in the presynaptic cell contribute to the transmission characteristics, e.g., by actively propagating the action potential to the site of electrical coupling (cf. Galarreta and Hestrin, 1999), or would a passive, action potential-like voltage waveform applied to the soma of the presynaptic cell evoke an identical postsynaptic response?

In order to examine the possible involvement of TTX-sensitive voltage-gated currents, we first recorded a series of electrical PSPs evoked by spontaneous presynaptic action potentials in the control condition (Figures 6A and 6C). Adding TTX blocked both action potentials and accompanying electrical PSPs (Figure 6B). We then changed the recording configuration of the presynaptic cell from current clamp to voltage clamp and applied a previously recorded action potential as a voltage-clamp command. The presynaptic voltage command waveform evoked postsynaptic depolarizations that

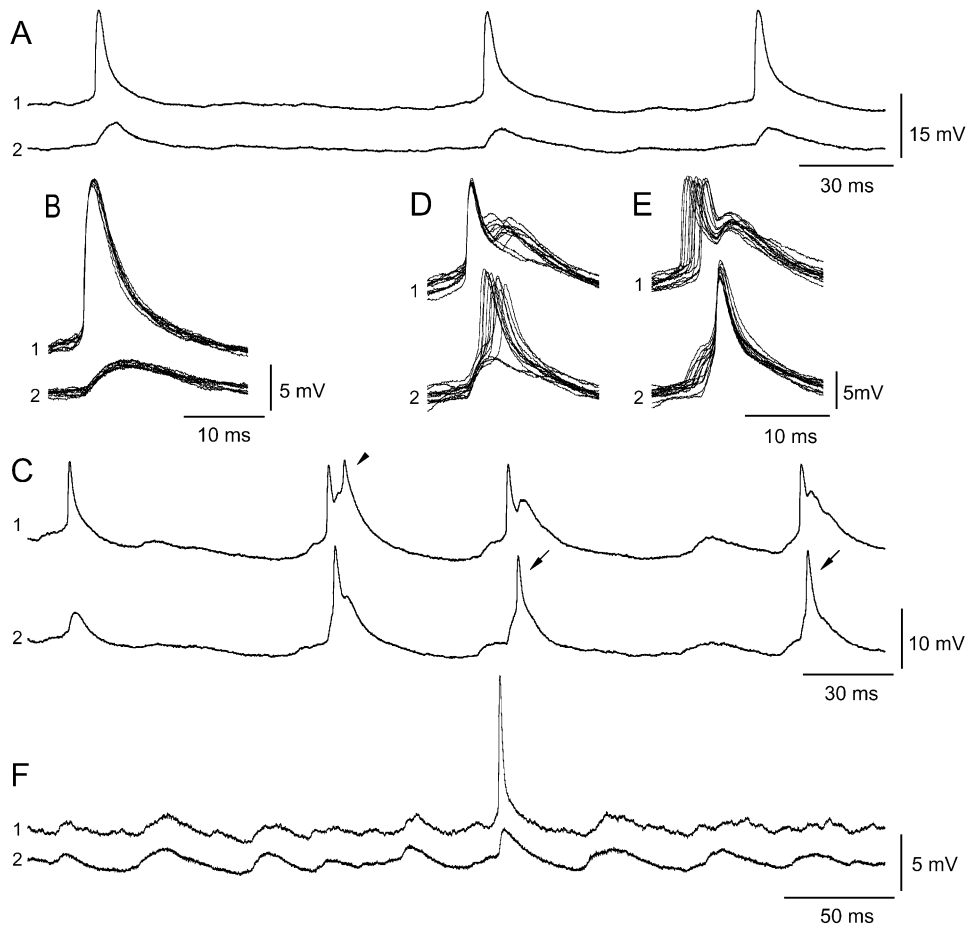


Figure 5. Electrical Postsynaptic Potentials (PSPs) in All Amacrine Cells

(A) Spontaneous activity of two simultaneously recorded, electrically coupled All amacrine cells. Spikes in cell 1 occur together with slower, subthreshold depolarizations in cell 2.

(B) Ten spontaneous activity traces of cell 1 and cell 2 aligned by a spike in cell 1. Same cell pair as (A).

(C) Spontaneous activity of two simultaneously recorded, electrically coupled All amacrine cells. Spikes in cell 1 occur together with slower, subthreshold depolarizations in cell 2, but sometimes the depolarization of cell 2 reaches threshold for spiking (arrows) and evokes a subthreshold depolarization of cell 1. The depolarization of cell 1 can reach threshold for spiking (arrowhead) followed by a subthreshold depolarization of cell 2.

(D) Twelve spontaneous activity traces of cell 1 and cell 2 aligned by a spike in cell 1. Same cell pair as (C). Note the low variability of latency between a spike in cell 1 and a subthreshold depolarization in cell 2 and the larger variability between a spike in cell 1 and a spike in cell 2.

(E) As (D), but aligned by a spike in cell 2. Note the low variability of latency between a spike in cell 2 and a subthreshold depolarization in cell 1.

(F) Spontaneous activity of two simultaneously recorded, electrically coupled All amacrine cells. Note simultaneously occurring subthreshold depolarizations in cell 1 and cell 2, presumably evoked by activity in a few other cells independently electrically coupled to both cells. A spike in cell 1 evokes an additional subthreshold depolarization in cell 2.

were very similar to those evoked by spontaneous action potentials (Figure 6D). To quantify the comparison of postsynaptic depolarizations evoked by spontaneous action potentials (in the control condition) and those evoked by simulated action potentials (in the presence of TTX), four response parameters were measured: latency, coupling coefficient, 10%–90% rise time of the postsynaptic depolarization, and relative half-width (ratio between half-width of the postsynaptic potential and half-width of the action potential). There was no significant difference between the values of each of the four parameters compared between control and TTX conditions ($p > 0.16$; $n = 4$ –6 cell pairs; paired t test for each response parameter). This suggests that voltage-gated

I_{Na} in neither the pre- or postsynaptic cell influenced the coupling characteristics or the time course of the postsynaptic response. In conclusion, the transfer of signals between electrically coupled cells seems fully accounted for by a passive, electrotonic mechanism.

Electrical Coupling and Coincidence Detection

Previous studies of electrically coupled neocortical interneurons demonstrated that electrical coupling can facilitate simultaneous spiking in response to synchronous, subthreshold input (Galarreta and Hestrin, 1999). This is particularly interesting for the operational characteristics of the network of All amacrine cells because All amacrine cells coupled directly by gap junctions are

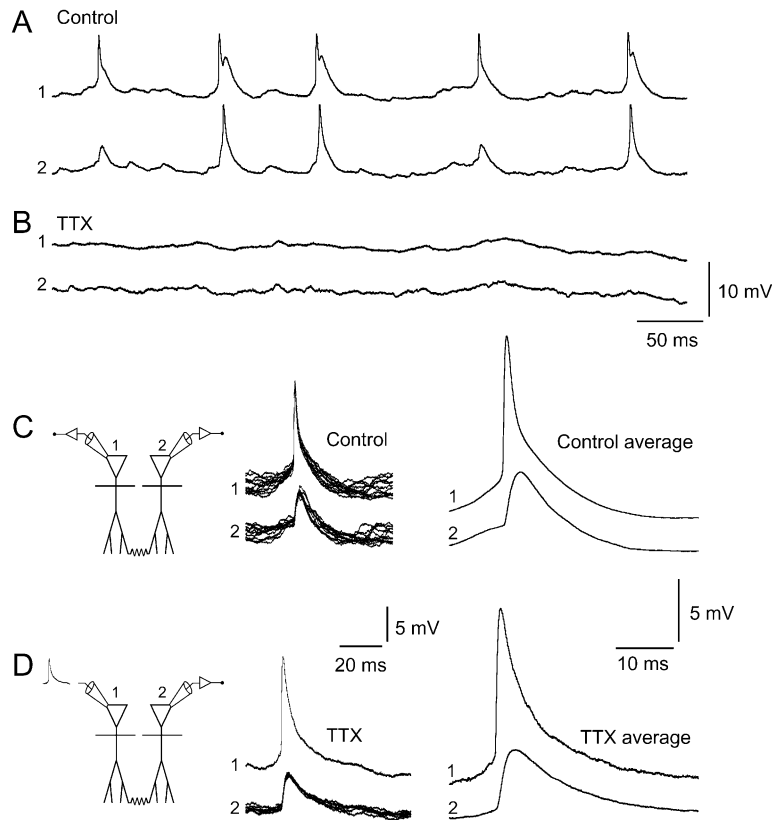


Figure 6. Passive Transmission of Action Potential Waveforms between Electrically Coupled All Amacrine Cells

(A) Spontaneous activity of two simultaneously recorded, electrically coupled All amacrine cells.

(B) TTX blocks spiking and corresponding subthreshold depolarizations.

(C) *Left*: recording configuration, both cells in current clamp. *Middle*: overlaid spontaneous activity (control) traces of cell 1 and cell 2 aligned by a spike in cell 1 ($n = 12$), only trace pairs when cell 2 did not reach spike threshold are included. *Right*: average of traces for cell 1 and cell 2.

(D) *Left*: recording configuration, cell 1 voltage clamped with pre-recorded action potential waveform and cell 2 in current clamp. *Middle*: overlaid evoked activity traces of cell 1 and cell 2 aligned by a simulated spike in cell 1 ($n = 7$). Recorded in the presence of TTX. *Right*: average of traces for cell 1 and cell 2. Note low variability and similarity of postsynaptic responses in (C) and (D). Same scales for middle and right panels in (C) and (D), respectively.

likely to receive common synaptic input from rod bipolar cells (Strettoi et al., 1992). We tested this by recording from pairs of cells in current clamp (chemical synaptic transmission blocked pharmacologically). Application of brief, subthreshold depolarizing current pulses to each cell resulted in a low firing probability when the current pulses were applied asynchronously (Figure 7). When identical current pulses were delivered synchronously to the cells, however, there was a clear increase in the firing probability (Figure 7). This result was observed in 10 of 10 cell pairs. For cells receiving asynchronous pulses, the average number of action potentials evoked by the current stimulus was 0.25 and for cells receiving synchronous pulses the average was 1.38 ($p = 0.00015$; $n = 20$ cells; paired t test).

Subthreshold Membrane Potential Synchronization and Oscillation

The temporally precise synchronization observed in the spike crosscorrelograms does not in itself reveal the existence or extent of subthreshold membrane potential synchronization (cf. Lampl et al., 1999). One possibility is that subthreshold membrane potential fluctuations in cells with correlated spiking are uncorrelated for longer periods of time, but interrupted by brief synchronous periods related to spike firing. Alternatively, subthreshold membrane potential fluctuations could be highly correlated for long, continuous periods of time, independent of correlated spiking. To examine this question quantitatively, we constructed sliding-window, 2D crosscorrelograms between pairs of simultaneously recorded

All amacrine cells. The 2D crosscorrelograms in Figure 8B were calculated from 15 s long continuous voltage records from a pair of electrically coupled cells (Figure 8A) and show strong, continuous synchronization of membrane potential fluctuations, both in the control condition (Figure 8A, top and Figure 8B, left) and after blocking chemical synaptic transmission pharmacologically (Figure 8A, bottom and Figure 8B, right). The time-averaged crosscorrelogram for each condition is shown in Figure 8C (left, black traces; top row control, bottom row with pharmacological blockers). To analyze the 2D crosscorrelograms in more detail, we calculated the peak amplitude, peak location (relative to zero time delay), and half-width duration of each (1D) crosscorrelogram as a function of recording time. For both recording conditions, the variability in synchrony over time was minimal with mean values of 0.57 ± 0.007 in control and 0.67 ± 0.007 with pharmacological blockers. The peak amplitude of the time-averaged crosscorrelograms was located very close to zero time delay (Figure 8C, left, black traces) and there was little fluctuation in the location of the peak as a function of time (Figure 8B). This indicates a consistent, near-zero time shift between the membrane potential fluctuations in the two cells and that moment-to-moment variations of membrane potential can be synchronous on a time scale of milliseconds. The half-width duration of the central peak of each crosscorrelogram displayed moderate variability (control: 34.0 ± 1.8 ms; with blockers: 26.8 ± 0.9 ms). 2D crosscorrelograms were constructed for a total of 17 cell pairs in the control condition and 26 cell pairs in the presence of blockers of chemical synaptic transmission. The aver-

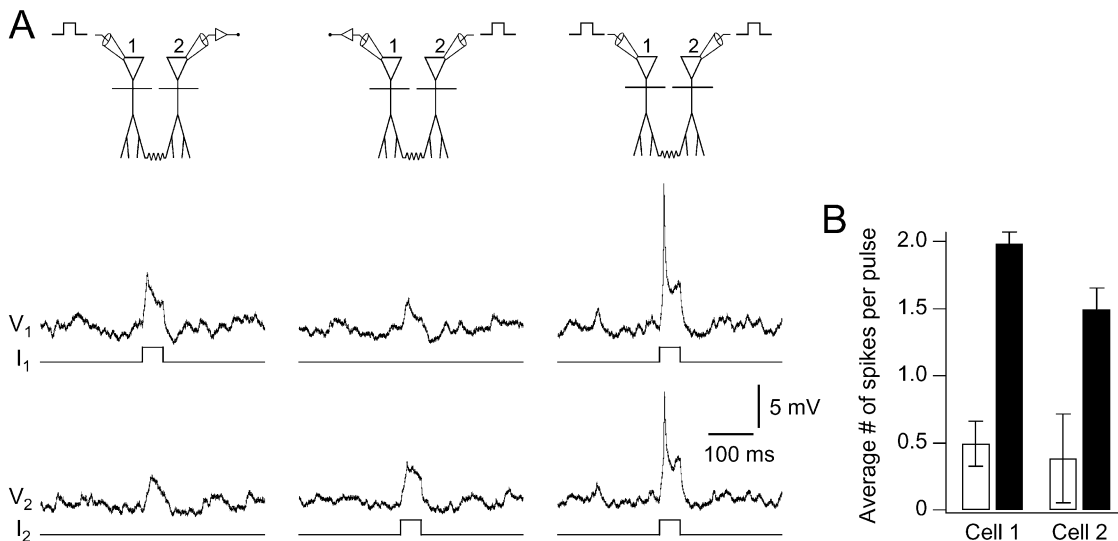


Figure 7. Electrical Coupling Facilitates Simultaneous Spiking in Response to Synchronous Subthreshold Input
(A) Subthreshold current pulse (14 pA, 50 ms) injected either asynchronously in each cell of a pair of electrically coupled All amacrine cells or synchronously to both cells.
(B) Bar graph representing average number of spikes per current pulse (same cell pair as in [A], 63 repetitions, open bars for asynchronous pulses, filled bars for synchronous pulses).

age peak amplitude was 0.56 ± 0.04 (range 0.21–0.76) in control and 0.61 ± 0.04 (range 0.22–0.98) with blockers. The average location of the peak (absolute value) was 3.1 ± 0.9 ms (range 0.1–14.4 ms) in control and 2.7 ± 0.4 ms (range 0.1–6.3 ms) with blockers. The average half-width was 40.4 ± 2.8 ms (range 12.1–64.5 ms) in control and 35.3 ± 3.4 ms (range 12.9–81.1 ms) with blockers. For each result, a comparison between the results in control condition and in the presence of blockers of chemical synaptic transmission indicated that there was no statistically significant difference ($p > 0.27$). For five cell pairs recorded under both conditions, a paired comparison confirmed no statistically significant difference between the same parameters ($p > 0.21$, paired *t* tests). As a control, we constructed shuffled crosscorrelograms with segments for the second cell chosen in random order with respect to the first cell (LampI et al., 1999). Additionally, crosscorrelograms were constructed from five pairs of All amacrine cells that were not electrically coupled. In no case did we observe consistent peaks in the shuffled (Figure 8C, left, red traces) or the noncoupled crosscorrelograms.

For most cell pairs, the crosscorrelograms indicated that the strong synchronization was accompanied by markedly oscillatory membrane potential fluctuations, both in the control condition (Figure 8C, top: middle and right) and when chemical synaptic transmission was blocked pharmacologically (Figure 8C, bottom: middle and right). In some cases, there was continuous oscillatory activity throughout the recording period. In other cases, the degree of oscillation varied over time with continuous synchronization alternating between oscillatory and non-oscillatory activity (Figure 8B), evidence of marked short-term dynamics in network activity. One type of oscillatory activity, occurring with relatively large amplitude, typically displayed a period of oscillation of 100–300 ms (Figure 8C, middle and right). Another type

of oscillatory activity was faster with a period of about 25–50 ms, corresponding to synchronously occurring electrical PSPs. Oscillatory activity was not blocked by replacing Ca^{2+} with Co^{2+} in the external solution ($n = 5$ cell pairs; data not shown), suggesting that it does not depend on unblocked neurotransmitter receptors, e.g., metabotropic glutamate receptors, or on intrinsic voltage-gated Ca^{2+} currents. Blocking voltage-gated Na^{+} channels by addition of TTX abolished electrical PSPs and the corresponding fast oscillations, but did not abolish the slower oscillations ($n = 7$ cell pairs; data not shown).

Discussion

We have presented physiological evidence demonstrating the existence of significant electrotonic coupling between All amacrine cells. The bidirectional, nonrectifying electrical synapses mediate sign-conserving signaling and promote synchronous subthreshold membrane potential fluctuations and spiking. This indicates a unique mode of operation and integrative capability of the interneuronal network of All amacrine cells. Importantly, the experiments were performed in mature tissue, thus excluding the possibility that the observations are unique to a particular developmental stage in maturation of the neuronal tissue.

Gap Junctions between All Amacrine Cells as Electrical Synapses

There is strong morphological evidence for gap junctions (with corresponding tracer coupling) between All amacrine cells and between All amacrine cells and presumed ON-cone bipolar cells, and there is evidence that the extent of tracer coupling is under modulatory control (reviewed by Vaney, 1997). Dye or tracer coupling is often used as an indicator of the presence of gap junc-

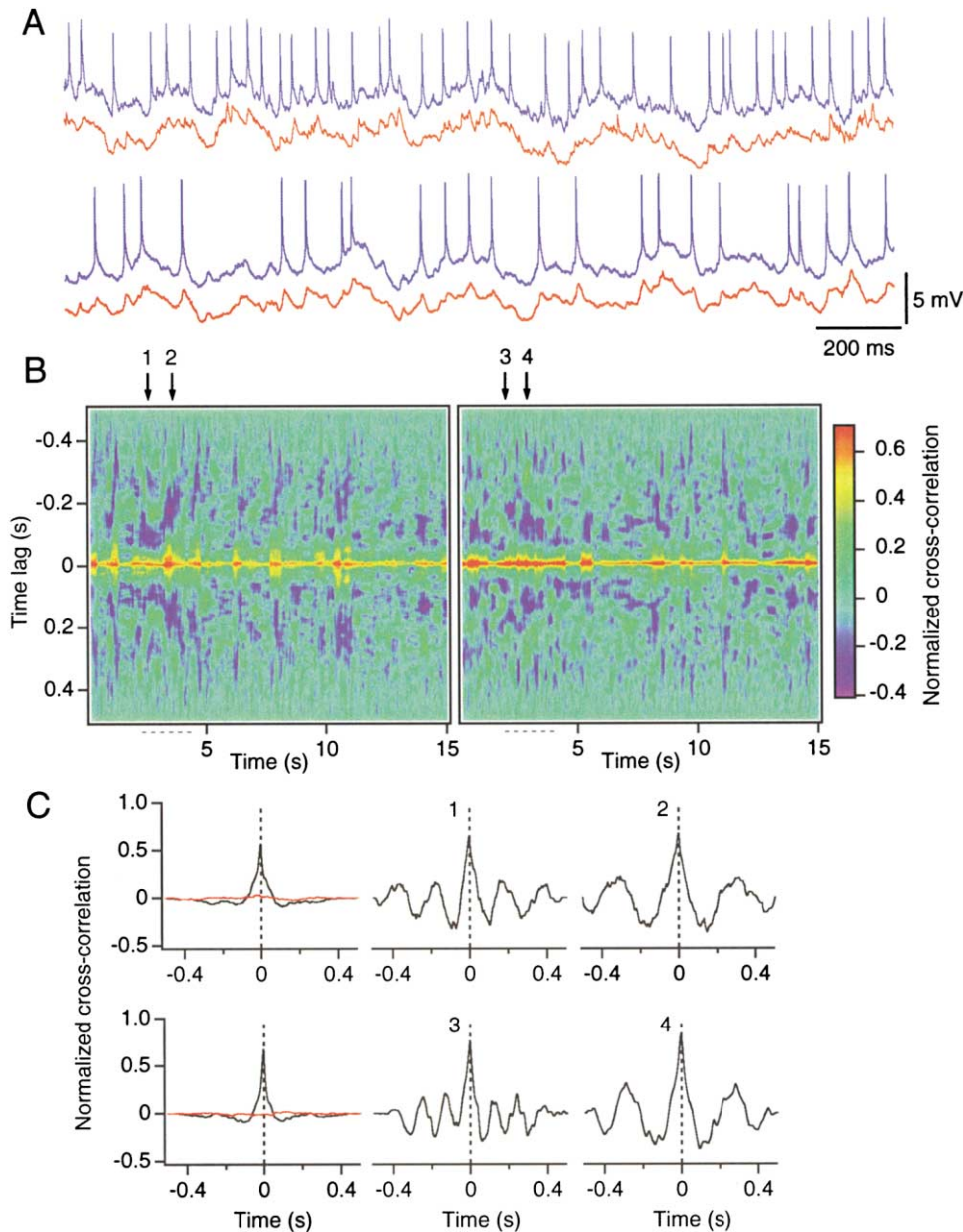


Figure 8. Synchronous Subthreshold Membrane Potential Fluctuations during Both Oscillatory and Non-Oscillatory Activity

(A) Spontaneous activity of a pair of simultaneously recorded, electrically coupled All amacrine cells (cell 1, red; cell 2, blue) in control solution (top) and in the presence of blockers of chemical synaptic transmission (bottom).

(B) Sliding 2D crosscorrelograms for 15 s continuous recordings of same cell pair as in (A) (left: control condition; right: in the presence of blockers of chemical synaptic transmission). Horizontal axis, time at the center of the 0.5 s sliding window; vertical axis, time lag from the center of the window (zero time delay). The normalized correlation amplitude coded by color (bar). Period of recordings in (A) indicated by dashed horizontal lines.

(C) One-dimensional crosscorrelograms (top row: control condition; bottom row: in the presence of blockers of chemical synaptic transmission): time-averaged normal (black) and shuffled (red) crosscorrelograms (left); crosscorrelograms centered at time points corresponding to arrows 1 (middle) and 2 (right) in (B) (control condition); crosscorrelograms centered at time points corresponding to arrows 3 (middle) and 4 (right) in (B) (with blockers).

tions between neurons, but is not direct evidence of electrical coupling. Several lines of evidence suggest that the observed electrical coupling between All amacrine cells is due to flow of current through gap junctions (and not an experimental artifact of the slice preparation, cf. Mann-Metzer and Yarom, 1999). First, the observed responses have the functional properties expected for

electrical coupling mediated by gap junctions (see above). Second, strong electrical coupling was only observed between cells whose processes were in potential physical contact with each other, as evidenced by fluorescence microscopy. Third, we never observed electrical coupling between All amacrine cells and other amacrine cells, irrespective of whether the cells were in

potential physical contact or not. Taken together, it is highly likely that the electrical coupling characterized in the present study is mediated by the gap junctions known to exist between All amacrine cells.

There is evidence that the neuron-specific connexin 36 (Cx36) is expressed by All amacrine cells and might be the subunit of All-All connexons (Feigenspan et al., 2001; Mills et al., 2001). If we assume that the gap junctions between these cells are homomeric and homotypic, the reported single-channel conductance of Cx36 connexons (14.3 pS; Teubner et al., 2000) allows us to estimate a lower limit for the number of gap junction channels between All amacrine cells. The highest junctional conductance was 1460 pS, corresponding to approximately 100 channels. Given that the open probability is likely to be less than unity, the true number of channels must be higher than this.

Electrical Coupling of All Amacrine Cells

The electrical junction conductance was highly symmetric, with no evidence for rectification. Asymmetrical coupling coefficients were well explained by corresponding differences in membrane input resistance. Consistent with results from other systems, electrical synapses between All amacrine cells displayed the functional characteristics of a low-pass filter. For steady state signals, we found coupling coefficients up to approximately 65%. For higher frequency signals, like action potentials, coupling coefficients were lower (3%–40%). It has been suggested that if presynaptic action potentials could be actively propagated (cf. Martina et al., 2000) from their site of generation towards the site of electrical coupling, the attenuation caused by passive propagation over the same distance would be counteracted (Galarreta and Hestrin, 1999, 2001). Accordingly, the coupling coefficient across the electrical synapses would be enhanced, compared to the expected coupling strength based on an electrotonic mechanism alone. Unfortunately, for All amacrine cells, it is not known where the voltage-gated Na^+ channels are located, where the action potentials are generated, or how they propagate. By employing pre-recorded action potentials as voltage-clamp templates, we could compare waveform parameters for electrical PSPs evoked by spontaneous and simulated spikes, the latter in the presence of TTX to block voltage-gated Na^+ channels. Importantly, the waveform parameters were very similar for the two cases. This does not exclude the possibility that naturally occurring action potentials propagate to, or arise close to, the site of electrical coupling in All amacrine cells, but suggests that if this the case, it does not constitute a mechanism of amplification of electrical synaptic transmission. A postsynaptic site of amplification would involve intrinsic currents that directly amplified the depolarization evoked by a presynaptic spike. Except for the case when an electrical PSP reaches spiking threshold, our results do not support the existence of such a mechanism. It is possible that the relatively small size of All amacrine cells reduces the effects of dendritic filtering and therefore the need for amplification of signal transmission.

Functional Consequences of Electrical Synapses between All Amacrine Cells

The focus on the functional importance of gap junction coupling between neurons in the rod pathway has pri-

marily been on fast excitatory transmission of signals from All amacrine cells to ON-cone bipolar cells. The present study suggests that temporally precise synchronization of activity among All amacrine cells could be of equal importance, both with respect to spiking and subthreshold membrane potential fluctuations. Indeed, electrical synapses are a common mediator of synchronized activity in neural networks and they are considered particularly effective in synchronizing subthreshold membrane potential fluctuations and oscillations (Galarreta and Hestrin, 2001).

The synchronization of spiking and subthreshold membrane potential fluctuations in electrically coupled All cell pairs occurred in both the presence and absence of spontaneous excitatory and inhibitory chemical synaptic input. The synchronization is most likely generated and maintained by the network of electrically coupled All amacrine cells. To our knowledge, there is no evidence for chemical inhibitory synapses between All amacrine cells. This contrasts with other networks of inhibitory interneurons where the cells can be reciprocally interconnected via both electrical and chemical (inhibitory) synapses (Galarreta and Hestrin, 1999; Gibson et al., 1999; Tamás et al., 2000; Bartos et al., 2001). Nevertheless, because All amacrine cells coupled by gap junctions are likely to receive common input from rod bipolar cells (Strettoi et al., 1992), it is likely that under natural conditions, electrical coupling will interact with excitatory chemical input to promote synchrony between All amacrine cells.

An important question raised by the present results concerns the control of the lateral spread of signals in the network of electrically coupled All amacrine cells. For example, one could envision that under some conditions, a spike in one cell might be propagated through electrical synapses all the way across the retina. The lateral extent of spike synchronization, as well as that of subthreshold membrane potential synchronization, is currently unknown. It is likely that lateral spread of signals is controlled by (at least) two mechanisms. First, inhibitory chemical synapses are located in close proximity to gap junctions at arboreal dendrites of All amacrine cells (Strettoi et al., 1992). Accordingly, the possibility should be considered that activation of this inhibitory input could functionally decouple select electrical junctions. Second, the electrical junction conductance could be directly modulated through activation of intracellular second messenger systems. Dynamic adjustment of these mechanisms could modulate and control the integrative properties of the network of All amacrine cells, including the lateral spread of active and passive signals, and thereby set the balance between sensitivity and spatial resolution in the rod system. Electrical coupling among inhibitory interneurons has also been suggested to be a substrate for coincidence detection, i.e., the ability of neurons to respond more readily to synchronous inputs (Galarreta and Hestrin, 1999; Bartos et al., 2001). The results reported here suggest that electrical coupling between All amacrine cells could serve a similar functional role (cf. Smith and Vardi, 1995).

For most cell pairs, the temporally precise synchronization of subthreshold membrane potential fluctuations displayed oscillatory behavior, both in control solution and after blocking chemical synaptic transmission pharmacologically. The oscillatory synchronization was not

abolished by blocking voltage-gated TTX-sensitive Na^+ channels or Co^{2+} -sensitive Ca^{2+} channels. The mechanisms responsible for generating these oscillations are unclear. It is not known if isolated All amacrine cells display membrane potential oscillations. Interestingly, however, several mechanisms have been proposed by which electrical coupling of intrinsically non-oscillatory cells can generate synchronous membrane potential oscillations (e.g., Loewenstein et al., 2001). The synchronous membrane potential oscillations of All amacrine cells could be of functional importance for the computations performed by this network of neurons and might directly influence OFF- and ON-cone bipolar cells via chemical and electrical synapses.

Experimental Procedures

Electrophysiology

Albino rats (4–7 weeks postnatal) were deeply anesthetized with halothane in oxygen and killed by cervical dislocation (procedure approved under the surveillance of the Norwegian Animal Research Authority). For a detailed account of the methods, including preparation of retinal slices, see Hartveit (1996).

The extracellular perfusing solution was continuously bubbled with 95% O_2 –5% CO_2 and had the following composition (in mM): 125 NaCl, 25 NaHCO_3 , 2.5 KCl, 2.5 CaCl_2 , 1 MgCl_2 , 10 glucose, pH 7.4 (20°C–24°C). In some experiments, we used an extracellular solution with low Ca^{2+} (0.15 mM) and high Mg^{2+} (3.35 mM). The recording pipettes (resistance 5.5–6.5 M Ω) were filled with a solution containing (in mM): 140 K-gluconate, 5 HEPES, 1 CaCl_2 , 1 MgCl_2 , 5 EGTA, 4 disodium adenosine 5'-triphosphate (Na_2ATP). Lucifer yellow was added (1 mg/ml) and pH was adjusted to 7.3 with KOH. The holding potentials were corrected for liquid junction potentials.

Drugs were added directly to the external solution. The concentrations of the drugs were as follows (in μM ; supplied by Tocris Cookson, Bristol, UK, unless otherwise noted): 30 3-(RS)-2-carboxypiperazin-4-yl-propyl-1-phosphonic acid (CPP), 10 6-cyano-7-nitroquinoxaline-2,3-dione (CNQX), 10 bicuculline methchloride, 1 strychnine (Research Biochemicals, Natick, MA), 0.3 tetrodotoxin.

Dual whole-cell recordings were made with an EPC9/2 amplifier (HEKA elektronik, Lambrecht, Germany). Cells were generally held at a membrane potential of -60 mV. The fast current-clamp feedback circuitry of the EPC9/2 was used in all current-clamp recordings. For some voltage-clamp experiments, the DAC-stimulus template corresponded to the digitization of a previously recorded action potential. Assuming that the low-pass filtering imposed by the combination of series resistance ($R_s = 10$ – 20 M Ω) and cell membrane capacitance (C_m ; appr. 15 pF) can be represented as a simple RC-filter ($f_c = 1/2\pi R_s C_m$), the voltage waveform imposed on the cell body would only be minimally distorted because of the relatively low amplitude and slow time course of the action potentials. The digital sampling interval was varied between 10 and 50 μs and the signal was low-pass filtered with a corner frequency (-3 dB) $1/3$ – $1/5$ of the inverse of the sampling interval. The cell membrane capacitance (C_{slow}) was estimated by the automatic capacitance neutralization network feature of the EPC9/2. For each measurement, the test pulse stimuli were sent simultaneously to both amplifiers in order to eliminate junctional currents. With this method, the average capacitance in the whole-cell recordings was 15.6 ± 0.3 (SEM) pF ($n = 76$). The series resistance in both cells was regularly monitored by applying a series of 10 mV hyperpolarizing voltage pulses (16 ms duration). The C_{slow} neutralization circuitry of the EPC9/2 was transiently disabled and the stimulus was sent to both amplifiers simultaneously. The average series resistance was 17 ± 1.0 (SEM) M Ω ($n = 76$). Cells with series resistance above 40 M Ω were excluded from analysis.

Data Analysis

Analysis was performed with PulseFit (HEKA elektronik), Igor Pro (WaveMetrics, Lake Oswego, OR), AxoGraph (Axon Instruments, Union City, CA), and DataView (Dr. W.J. Heitler, University of St. Andrews, UK).

In order to calculate the steady-state electrical junction conductance (G_j), we assumed an equivalent-circuit model and corrected for errors introduced by nonzero R_s and finite membrane resistance (R_m ; Van Rijen et al., 1998). Discrete crosscorrelations were determined from trains of action potentials by calculating the temporal interval from the time of occurrence of each action potential in the reference cell to the time of occurrence of all action potentials in the nonreference cell. The intervals were binned (1 ms resolution) and used to generate a crosscorrelation histogram where the value of each bin indicated the number of action potentials that occurred in the nonreference cell. For two neurons firing randomly, the expected level of correlation was calculated as: $N_1 \times (1/T) \times b \times N_2$, where N_1 is the total number of spikes in the nonreference cell, T is the duration over which the spikes occurred, b is the bin width, and N_2 is the total number of spikes in the reference cell. The expected level of correlation corresponded very well with results obtained from shuffled crosscorrelograms (constructed after adding 1 s to the spike times of one of the cells in a pair). The synchronization width was defined as the width of the crosscorrelogram peak at the 99% confidence level (Mann-Metzer and Yarom, 1999). Synchronization strength was calculated as the integral of the crosscorrelogram peak over the synchronization width divided by the corresponding integral limited by the expected level of correlation (cf. Mann-Metzer and Yarom, 1999; Brivanlou et al., 1998). The time delay of the central peak of each spike crosscorrelogram was determined from a fit by a Gaussian function of the form (Brivanlou et al., 1998): $R = b + ae^{-(t-d)^2/2w^2}$, where b is the baseline firing rate, a is the amplitude of the peak, w is the standard deviation of the peak, and d is the delay of the peak relative to zero time delay.

Normalized crosscorrelograms of continuous membrane potential recordings were calculated as the correlation of the two records divided by the number of points and the standard deviation of each voltage record. Accordingly, the crosscorrelation amplitude depends only on the degree of synchrony between the voltage records and not on their absolute amplitude. Sliding, color-coded two-dimensional (2D) crosscorrelograms of pairs of voltage records of duration T s were calculated from N consecutive pairs of data segments, each of duration T/N s and shifted 100 ms forward in time relative to the previous segment. Each segment was mean-subtracted before calculating the crosscorrelation, which is therefore mathematically equivalent to the crosscovariance. A matrix was then constructed where consecutive 1D crosscorrelation functions constitute consecutive columns with time running along the x axis and the time lag of the correlation function running along the y axis. The normalized correlation amplitude was coded by color. The time-averaged crosscorrelogram was calculated as the average of each row of the 2D crosscorrelogram.

Statistical analyses were performed with Student's two-tailed t tests with a level of significance of $p < 0.05$ (unpaired, unless otherwise stated). Data are presented as means \pm SEM (n = number of cells or cell pairs).

Acknowledgments

We thank Dr. W.J. Heitler for generous help with offline analysis of paired recordings. Financial support from the Norwegian Research Council (NFR 123487/310, 129566/310, 123485/310, 141392/310) and the Meltzer fund (University of Bergen) is gratefully acknowledged.

Received: October 26, 2001

Revised: January 14, 2002

References

- Bartos, M., Vida, I., Frotscher, M., Geiger, J.R.P., and Jonas, P. (2001). Rapid signaling at inhibitory synapses in a dentate gyrus interneuron network. *J. Neurosci.* 21, 2687–2698.
- Boos, R., Schneider, H., and Wässle, H. (1993). Voltage- and transmitter-gated currents of All-amacrine cells in a slice preparation of the rat retina. *J. Neurosci.* 13, 2874–2888.
- Brivanlou, I., Warland, D.K., and Meister, M. (1998). Mechanisms of concerted firing among retinal ganglion cells. *Neuron* 20, 527–539.
- Feigenspan, A., Teubner, B., Willecke, K., and Weiler, R. (2001).

- Expression of connexin36 in All amacrine cells of the mammalian retina. *J. Neurosci.* 21, 230–239.
- Galarreta, M., and Hestrin, S. (1999). A network of fast-spiking cells in the neocortex connected by electrical synapses. *Nature* 402, 72–75.
- Galarreta, M., and Hestrin, S. (2001). Electrical synapses between GABA-releasing interneurons. *Nat. Rev. Neurosci.* 2, 425–433.
- Gibson, J.R., Beierlein, M., and Connors, B.W. (1999). Two networks of electrically coupled inhibitory neurons in neocortex. *Nature* 402, 75–79.
- Hartveit, E. (1996). Membrane currents evoked by ionotropic glutamate receptor agonists in rod bipolar cells in the rat retinal slice preparation. *J. Neurophysiol.* 76, 401–422.
- Kolb, H., and Famiglietti, E.V. (1974). Rod and cone pathways in the inner plexiform layer of cat retina. *Science* 186, 47–49.
- Lampl, I., Reichova, I., and Ferster, D. (1999). Synchronous membrane potential fluctuations in neurons of the cat visual cortex. *Neuron* 22, 361–374.
- Loewenstein, Y., Yarom, Y., and Sompolinsky, H. (2001). The generation of oscillations in networks of electrically coupled cells. *Proc. Natl. Acad. Sci. USA* 98, 8095–8100.
- Mann-Metzer, P., and Yarom, Y. (1999). Electrotonic coupling interacts with intrinsic properties to generate synchronized activity in cerebellar networks of inhibitory interneurons. *J. Neurosci.* 19, 3298–3306.
- Martina, M., Vida, I., and Jonas, P. (2000). Distal initiation and active propagation of action potentials in interneuron dendrites. *Science* 287, 295–300.
- Masland, R.H. (2001). The fundamental plan of the retina. *Nat. Neurosci.* 4, 877–886.
- Mills, S.L., O'Brien, J.J., Li, W., O'Brien, J., and Massey, S.C. (2001). Rod pathways in the mammalian retina use connexin 36. *J. Comp. Neurol.* 436, 336–350.
- Nolan, M.F., Logan, S.D., and Spanswick, D. (1999). Electrophysiological properties of electrical synapses between rat sympathetic preganglionic neurones in vitro. *J. Physiol.* 519, 753–764.
- Smith, R.G., and Vardi, N. (1995). Simulation of the All amacrine cell of mammalian retina: Functional consequences of electrical coupling and regenerative membrane properties. *Vis. Neurosci.* 12, 851–860.
- Strettoi, E., Raviola, E., and Dacheux, R.F. (1992). Synaptic connections of the narrow-field, bistratified rod amacrine cell (All) in the rabbit retina. *J. Comp. Neurol.* 325, 152–168.
- Tamás, G., Buhl, E.H., Lörincz, A., and Somogyi, P. (2000). Proximally targeted GABAergic synapses and gap junctions synchronize cortical interneurons. *Nat. Neurosci.* 3, 366–371.
- Teubner, B., Degen, J., Söhl, G., Güldenagel, M., Bukauskas, F.F., Trexler, E.B., Verselis, V.K., De Zeeuw, C.I., Lee, C.G., Kozak, C.A., et al. (2000). Functional expression of the murine connexin 36 gene coding for a neuron-specific gap junctional protein. *J. Membr. Biol.* 176, 249–262.
- Vaney, D.I. (1997). Neuronal coupling in rod-signal pathways of the retina. *Invest. Ophthalmol. Vis. Sci.* 38, 267–273.
- Van Rijen, H.V.M., Wilders, R., Van Ginneken, A.C.G., and Jongsma, H.J. (1998). Quantitative analysis of dual whole-cell voltage-clamp determination of gap junctional conductance. *Pflugers Arch.* 436, 141–151.